Optical properties of conjugated polymer-ZnSe nanocrystal nanocomposites*

Yun Da-Qin(云大钦)[a], Feng Wei(封 伟)[b]†, Wu Hong-Cai(吴洪才)[a], Liu Xiao-Zeng (刘效增)[a], and Qiang Jun-Feng(强军锋)[a]

[a] *School of Electrical and Information Engineering, Xi'an Jiaotong University, Xi'an* 710049, *China*

[b] *School of Materials Science and Engineering, Tianjin University,* 300072, *China and Tianjin Key Laboratory of Composite and Functional Materials, Tianjin* 300072, *China*

(Received 15 July 2009; revised manuscript received 4 August 2009)

Nanocomposites of poly[(2-methoxy,5-octoxy)1,4-phenylenevinylene]-zinc selenide (MOPPV-ZnSe) are synthesized by mixing the polymerization of 1,4-bis (chloromethyl)-2-methoxy-5-octoxy-benzene in the presence of ZnSe quantum dots. The resulting MOPPV-ZnSe nanocomposites possess a well-defined interfacial contact, thus significantly promoting the dispersion of ZnSe within the MOPPV matrix and facilitating the electronic interaction between these two components. Raman and UV–visible absorption spectra are influenced by the incorporation of ZnSe nanocrystals. High-resolution transmission electron microscopic and tapping-mode atomic force microscopic results show clearly the evidence for phase-segregated networks of ZnSe nanocrystals, which provide a large area of interface for charge separation to occur. Steady-state spectra of MOPPV-ZnSe nanocomposites are markedly quenched by the introduction of intimate polymer/ZnSe junctions. Time-resolved photoluminescence measurements show that the lifetime decays quickly, which further confirms the occurrence of charge transfer in MOPPV-ZnSe nanocomposites.

Keywords: nanocomposites, interface, time-resolved photoluminescence spectrum, excitons separation

PACC: 7340, 7860, 8140T

1. Introduction

In recent years photovoltaic devices based on solution-processing semiconductor nanocrystal-conjugated polymer composites have been significantly improved in efficiency.[1−6] The superior efficiency of hybrid photovoltaic devices over neat-polymer-based ones arises from the efficient dissociation of excitons at the polymer-semiconductor nanocrystal interface, thereby providing continuous pathways for electrons and holes to be efficiently transported into the electrodes within the acceptor and donor materials before the occurrence of recombination, separately. Therefore, the conversion of excitons into charge carriers at the polymer-semiconductor interface is a key step to hybrid photovoltaic devices, which is strongly dependent on the degree of interfacial contact. Typically, semiconductor nanocrystals are directly blended with the polymers at an appropriate concentration in order to optimize the interfacial contacts and promote the formation of percolation pathways for charge transport. The mixing approach requires the use of co-solvents, which in turn affects nanocrystal solubility and polymer chain orientation and inefficiently photoinduces charge-separation and charge-transport processes for photovoltaic devices. Moreover, it is considerably noteworthy that conjugated polymers are generally hydrophobic, whereas inorganic nanocrystals are hydrophilic. Bartholomew and Heeger have reported the infiltration of regioregular poly(3-hexylthiophene) (P3HT) in a random nanocrystalline TiO_2 network. However, they observed a very low level of polymer incorporation (∼0.5%), even for highly porous (∼65%) networks.[7] As a result, the hydrophilicity mismatch causes another critical problem for the interfacial contacts. On the basis of the problems mentioned above, it is still a challenge to produce polymer-nanocrystal nanocomposites which are well dispersed to obtain intimate interfacial contacts. However, relatively few studies have concentrated on the direct integration of semiconductor nanocrystals into conjugated polymers by

*Project supported by the National Natural Science Foundation of China (Grant No. 50873074), Program for New Century Excellent Talents in University of Chinese Education Ministry (Grant No. 060232), Foundation for Key Program of Ministry of Education, China (Grant No. 108029) and Scientific Research Foundation of Xi'an Jiaotong University, China (Grant No. 011092).

†Corresponding author. E-mail: weifeng@tju.edu.cn

© 2010 Chinese Physical Society and IOP Publishing Ltd

the direct polymerization method to achieve a more controlled interface and morphology.[8−10]

In the present study, we present the preparation of poly[(2-methoxy,5-octoxy)1,4-phenylenevinylene]-zinc selenide (MOPPV-ZnSe) nanocomposites in different weight ratios by the mixing polymerization method. We observe steady state and the time-resolved photoluminescence (PL) quenching and charge transfer occurring at the polymer-ZnSe nanocrystal interface. The properties and the morphology of nanocomposite are also demonstrated in detail, based on their optical and structural characterizations with Raman and UV–vis absorption spectra, as well as high resolution transmission electron microscopy (HRTEM) and tapping-mode atomic force microscopy (TM-AFM).

2. Experimental section

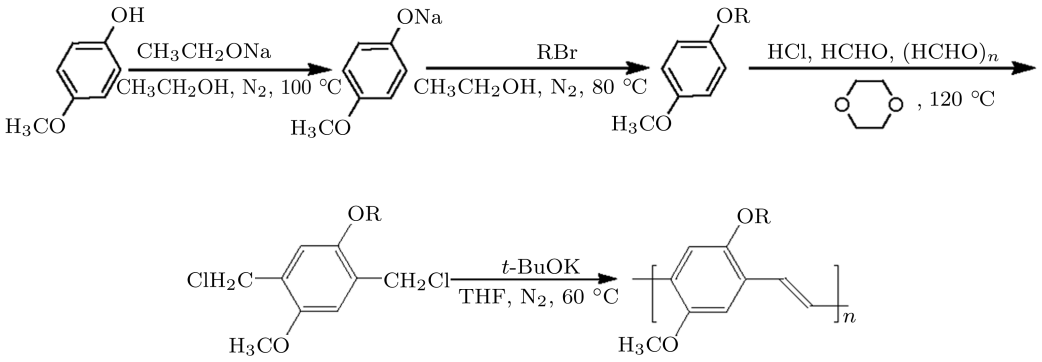
All reagents used in the present experiment are available commercially unless otherwise stated. Tetrahydrofuran (THF) was distilled from sodium benzophenone prior to use.

2.1. Synthesis of ZnSe quantum dots

The preparation of ZnSe quantum dots (QDs) was performed in our laboratory according to a reported method.[11] Briefly, Se powder was reduced fast by excess sodium borohydride under N_2 atmosphere in a water and alcohol system at 70 °C for about 30 min. Secondly, excess 0.5 mol/dm^3 H_2SO_4 was introduced to generate H_2Se gas that was absorbed in turn by the NaOH aqueous solution. Thus, an aqueous solution of NaHSe was obtained. Then the NaHSe solution was incorporated into an oxygen-free $ZnCl_2$ solution at pH 6.5 in the presence of L-cysteine (L-cys) as the stabilizer. The molar ratio of Zn^{2+} : NaHSe : L-cys was equal to 1 : 0.5 : 2.4. Finally, ZnSe QDs grew by water-bath heating at 100 °C for a period from several hours to 2 days. Subsequently, the L-cys–coated quantum dot precipitate was separated by centrifugation and decantation. The precipitate was further dispersed and washed three times in chloroform and pyridine to remove the original surfactant, separately. The final product was dried under vacuum.

2.2. Synthesis of the monomer

We adopted a synthetic procedure similar to that in Ref. [12] for MOPPV to synthesize MOPPV-ZnSe nanocomposites as shown in Scheme 1. The precursor, 1,4-bis (chloromethyl)-2-methoxy-5-octoxy-benzene, was prepared in the way clearly described in our previous studies.[13] First, 1-methoxy-4-octoxy-benzene was synthesized from the reaction of 4-methoxyphenol with *n*-octyl bromide in the presence of $NaOCH_2CH_3$. Second, the monomer, 1,4-bis (chloromethyl)-2-methoxy-5-octoxy-benzene, was then prepared by the chloromethylation of its precursor in the system of formaldehyde, HCl and a little paraformaldehyde in dioxane solution.



R=$CH_2(CH_2)_6CH_3$

Scheme 1. Synthetic route to MOPPV.

2.3. Synthesis of the MOPPV-ZnSe nanocomposites

Briefly, to a round bottomed flask, well flushed with N_2 and equipped with a rheostat as the mechanical stirrer, was added a solution of potassium tert-butoxide in dry THF at 70 °C. A blend solution of monomers, namely 1,4-bis(chloromethyl)-2-methoxy-5-octoxy-benzene, and ZnSe quantum dots in dry THF were then added at a rate of 20 ml/h with a syringe pump. After the complete addition, the blend solution under reaction was stirred for 16 h. The reaction product was poured into rapidly stirred methanol, and the deposited matter was collected by suction filtration and then washed with a methanol/water mixture (1/1,volume/volume) three times to remove the by-product. The purified MOPPV-ZnSe nanocomposite product was dried under vacuum. Pure MOPPV was synthesized for comparative measurements according to the approach described above.

2.4. Measurements

TEM images were obtained by a JEOL JEM-3010 TEM at 100 keV. The samples for TEM were prepared by drop casting of a small quantity of the material on lacey or holey copper grids. TM-AFM image was obtained by using a Digital Instruments NanoScope III system to observe the areas of the device where no top electrode was deposited. Raman spectra were recorded by using an RM 2000 microscopic confocal Raman spectrometer (Renishaw PLC, England) with a 632.8 nm laser beam and a charge coupled device detector of 4-cm^{-1} resolution. The absorption spectra of the samples were measured with a Hitach 2000 UV–vis spectrophotometer. Steady-state and time-resolved PL measurements were performed at the Multiphase Flow Laboratory. Steady-state PL spectra were obtained under identical excitation conditions by using a PTI QM4 luminescence spectrometer. Monochromatic excitation light was generated by a xenon arc lamp with double monchromators. Fluorescence was collected by an R928 photomultiplier tube (PMT) at room temperature relative to the excitation beam passing through a single monochromator. Fluorescence decay signals were obtained by using the technique of time correlated single photon counting (TCSPC). The excitation source was a nitrogen pumped dye laser and a laser strobe fluorescence lifetime detector for measuring. The instrument response function (IRF) with a pulse width of 100 ps from this system was measured when the excitation wavelength was the same as the emission wavelength irradiating the film sample. The 1-4 exponential lifetime method was used to model the decay curves to reproduce the true decay kinetics.

3. Results and discussion

3.1. Transmission electron microscopy

Figure 1(a) shows an HRTEM image of a sample prepared from ZnSe QDs. The as-prepared ZnSe QDs of ∼3 nm diameter with nearly uniform sphericity were stabilized with capping surfactants. The selected area diffraction pattern (Fig. 1(a), top inset) displays the diffraction rings corresponding to (111), (220), (311) lattice planes of the zinc blende structure of ZnSe exclusively.

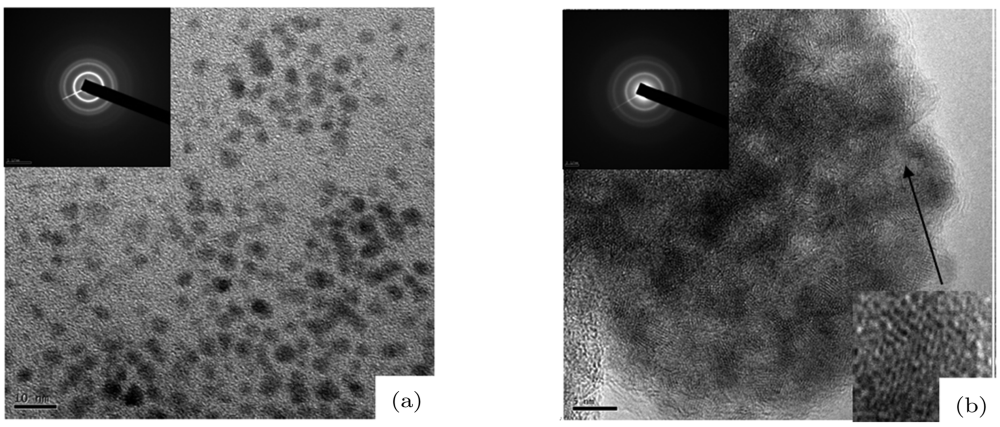


Fig. 1. (a) HRTEM image of ZnSe QDs and (b) HRTEM image of MOPPV-ZnSe nanocomposite with 50 wt% ZnSe, showing lattice structure (top inset) and crystalline nature of the ZnSe nanocrystals (bottom inset).

Figure 1(b) is an HRTEM image showing that the ZnSe nanocrystals of ∼4 nm diameter with high crystallinity (Fig. 1(b), bottom inset) are randomly distributed in the MOPPV host in chloroform solution with a ZnSe concentration of 50% in weight. From Fig. 1(b), we can also see that two components of the nanocomposite form a well-defined interface and an interpenetrating phase-separated (MOPPV) donor/acceptor (ZnSe) network. As a result, these results might provide a maximizing interface area for exciton dissociation and efficient conducting pathways to the electrode. Besides, comparing Fig. 1(b) with Fig. 1(a) above, we find that ZnSe QDs slightly grew during the mixing polymerization reaction and their radius changed from ∼3 nm to ∼4 nm in the polymer matrix. The selected area diffraction pattern (Fig. 1(b), top inset) shows diffraction rings corresponding to (111), (220), (311) lattice planes of the zinc blende structure of ZnSe exclusively.

3.2. Tapping-mode atomic force microscopy

The surface topography of MOPPV-ZnSe nanocomposite thin film was observed by TM-AFM as shown in Fig. 2. In general, a TM-AFM phase image can give the information about the height difference and also about the constituent of the nanocomposite thin film at the surface because the hard nanoparticle can easily be distinguished from the soft polymer. The phase shift of the cantilever oscillation is related to the power dissipated in a nonelastic tip phase shift with respect to a soft polymer, and hence the bright areas in Fig. 2 are interpreted as the harder nanoparticle (ZnSe) and the dark areas as the softer polymer (MOPPV). A feature of a better dispersion of ZnSe nanocrystal structure is found, which shows that more donor (MOPPV)-acceptor (ZnSe) interfaces are inevitably provided and their own networks in the active layer are formed. Moreover, the height image of the film exhibits clearly that the surface of the nanocomposite thin film is smooth (its root mean squared (RMS) roughness is only 0.743 nm). The results suggest that the interpenetrating network and the small feature size in the thin layer would conduce to more efficient exciton dissociation, provide more conducting paths for charge transfer and then lead to the improvement of device performance.

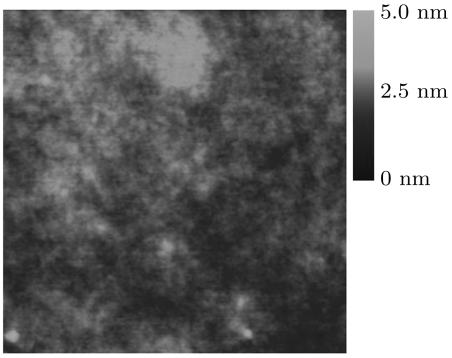


Fig. 2. Tapping-mode AFM phase image of the surface of the MOPPV-ZnSe nanocomposite thin film with a ZnSe concentration of 50 wt%. The image size is 1.1 μm×1.1 μm, and the vertical scale is 5.0 nm.

3.3. Raman spectra

Figure 3(a) shows the normalized Raman spectra with the excitation wavelength $\lambda_{\rm L}$ = 632.8 nm of MOPPV and MOPPV-ZnSe nanocomposites in the range 900–1800 cm^{-1}. From curve A in Fig. 3(a), the

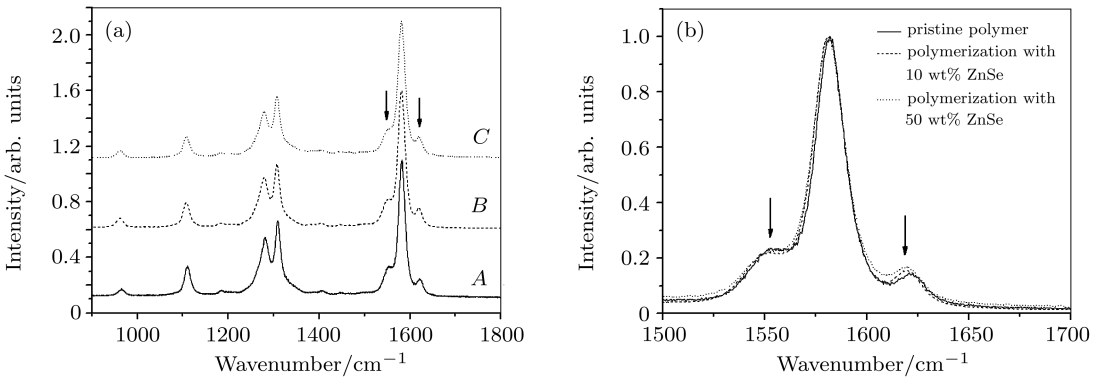


Fig. 3. (a) Raman spectra of the MOPPV and composites at room temperature for $\lambda_{\rm L}$ = 632.8 nm in the range 900–1800 cm^{-1} and (b) in the range 1500–1700 cm^{-1}. Curve *A* MOPPV (solid line); Curve *B* MOPPV-ZnSe (10 wt%) (dash line); Curve *C* MOPPV-ZnSe (50 wt%) (dot line).

band at 965 cm^{-1} is due to the out-of-plane C–H bending mode of the vinyl group. The band at 1111 cm^{-1} is assigned to the C–C stretching coupled to the CC–H bending mode of the phenyl ring. The bands at 1281 and 1310 cm^{-1} are related to a C=C stretching coupled to the CC–H bending mode of the vinyl group. The two bands at 1553 and 1582 cm^{-1} are associated with the C=C and C–C stretching vibrations of the phenyl ring, respectively. The band at 1621 cm^{-1} is assigned to a C=C stretching vibration of the vinyl group. The above characteristic Raman bands of the MOPPV are consistent with data reported in Ref. [14]. At the same time, the main features of the Raman spectra of nanocomposites are similar to those of MOPPV.

The main difference between the pristine polymer and its nanocomposites is the modification of the triplet peaks in the 1500–1700 cm^{-1} as shown in Fig. 3(b). The intensity ratio, I_{1553}/I_{1621}, is related to the conjugation length of the polymer.[15] When the conjugation length is reduced, the intensity of I_{1621} becomes stronger than that of I_{1553}. Therefore, a comparison between this ratio and that of the pure polymer (I_{1553}/I_{1621} ≈1.64) shows that this ratio has a weak decline i.e. I_{1553}/I_{1621}≈1.44 (10 wt% ZnSe and I_{1553}/I_{1621}≈1.31 (50 wt% ZnSe, which suggests that the introduction of ZnSe nanocrystals into MOPPV can reduce the conjugation length of the polymer chains, which is in agreement with the UV–vis absorption results.

3.4. UV–vis absorption spectra

We show the normalized UV–vis absorption spectra of ZnSe QDs, MOPPV, MOPPV-ZnSe polymerization and MOPPV/ZnSe blend composites in chloroform solution at room temperature in Fig. 4. It is evident that ZnSe QDs have a first exciton absorption peak at 320 nm (3.9 eV) and a significant blueshift with respect to the band gap energy of bulk ZnSe (2.7 eV).[16] Moreover, we notice that the broad absorption bands of MOPPV contain three peaks at 495, 329 and 294 nm, which should be assigned to the transitions of the 0–0, 0–1, and 0–2 vibronic structures, respectively.[15,17] Interestingly, compared with the pristine polymers, the MOPPV-ZnSe nanocomposites are only slightly blueshifted in the maximum peak and accompanied by a quantitatively correlated increase in optical absorption in a 260 nm–450 nm region. This blueshift clearly shows that the effective conjugation length of MOPPV is shortened with the increase of content of ZnSe nanocrsytals, which is attributed to the reduced aggregation of the polymer chains in the nanocomposites from the ZnSe nanocrystals barriers. The result is consistent with the results obtained from the analysis of the Raman spectra above. Additionally, the significant enhancement in optical absorption at around 290 nm in the MOPPV-ZnSe nanocomposites might be attributed to the augmented weight of the short segments in the MOPPV-ZnSe nanocomposites because the increase of the ZnSe nanocrystals percentage determines a further rise of short segment weight in the distribution. However, there is no evidence of significant structural change in absorption spectra for the MOPPV-ZnSe nannocomposites. This implies no significant ground state electronic or charge transfer interaction between the polymer and the ZnSe nanocrystals. On the other hand, it is also noteworthy that the spectrum of the MOPPV/ZnSe blend composite has no change in the position of the absorption peaks but it only resembles a superposition of the two components with no other apparent features present.

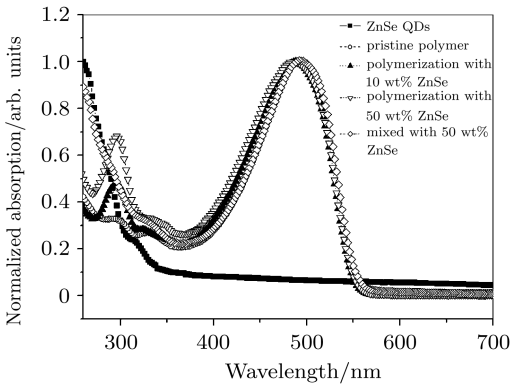


Fig. 4. Absorption spectra of ZnSe QDs, MOPPV, MOPPV-ZnSe polymerization and MOPPV/ZnSe blend composites in chloroform solution.

3.5. Steady-state PL

The electronic interactions in the excited states of MOPPV-ZnSe polymerization and MOPPV/ZnSe blend composition thin films were studied by means of PL spectra in Fig. 5. All thin films were deposited from the same solutions at the same concentrations and spin speeds, resulting in similar film thicknesses. When all films were excited at 350 nm, they emitted luminescence in a range of 550–700 nm with the maximum at 630 nm. It is noteworthy that there appear a larger decrease in luminescence intensity and a slightly blueshifted luminescence peak of the MOPPV-ZnSe nanocomposites. A comparison be-

tween the above absorption and the Raman spectra shows the slight blueshift of the PL peak, which further confirms that the presence of ZnSe nanocrystals reduces the effective π-conjugation length of MOPPV chains in the MOPPV-ZnSe nanocomposites. However, the photoluminescence of MOPPV/ZnSe (50 wt%) blend composite is not blueshifted but relatively low quenched compared with that of MOPPV-ZnSe (50 wt%) nanocomposite. This could be attributed to the easy formation of nanocrystal aggregation in the blend system due to the high surface-to-volume ratio of ZnSe nanoparticles thereby hindering the efficient dissociation of excitons between the MOPPV and ZnSe nanocrystals. PL quenching provides the evidence for charge transfer and exciton dissociation at the interface between the polymer and the nanocrystals. If the excitons are efficiently dissociated, direct exciton recombination is suppressed and thus the PL emission is significantly quenched. To further confirm the mechanisms, we need to carry out a time-resolved PL measurement.

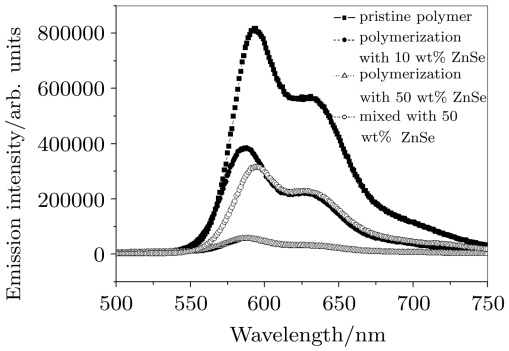


Fig. 5. Emission spectra of MOPPV, MOPPV-ZnSe polymerization and MOPPV/ZnSe blend thin films excited at 350 nm.

3.6. Time-resolved PL

To obtain a better understanding of how the presence of ZnSe nanocrystals affected the excited-state dynamics, time-resolved PL decays were measured for films on quartz. All thin films were deposited from the same solutions at the same concentrations and spin speeds, resulting in similar film thicknesses. In particular the observation of different lifetimes for the two emission peaks observed confirms that they did not originate from the same emissive state. We refer to the portion of the emission that has its intensity maximum near 590 nm as the 'blue' PL and the portion of the emission that peaks near 630 nm as the 'red' PL. The first emission peak (630 nm) reflects the lowest excited transition, while the second emission (590 nm) component should be attributed to the $S_2 \rightarrow S_0$ vibronic transition because the difference between their energies is approximately equal to that between the two lowest absorption peaks, which is in agreement with an earlier analysis of MOPPV polymer by Yang *et al.*[18] The decays fit to double and triple exponentials for pristine polymer and hybrid thin films, respectively. Average decay time was calculated to be the lifetime weighted by the yield for each exponential. Reduced chi-square for all fits is less than or equal to 1.2 and the Durbin–Watson parameter is greater than or equal to 1.7.

Figures 6 and 7 show the PL decay curves for the pristine MOPPV and the hybrid films as a function of concentration of ZnSe measured by pumping at 350 nm and probing at the 'blue' and the 'red' ends (590 nm and 630 nm), respectively. The analyses of their PL lifetime decays are summarized in Table 1 and Table 2, respectively. Firstly, it can clearly be seen in Tables 1 and 2 that the pure MOPPV layer

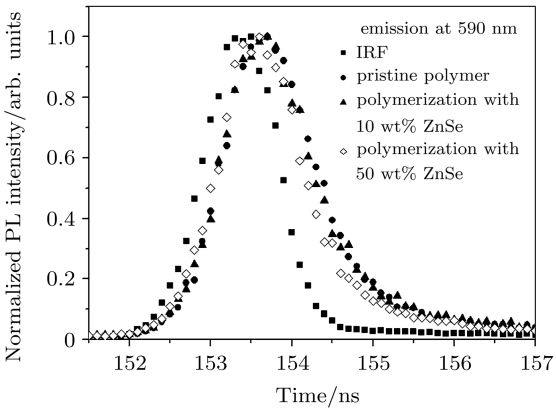


Fig. 6. Decay curves of the MOPPV and the MOPPV-ZnSe thin films excited at 350 nm.

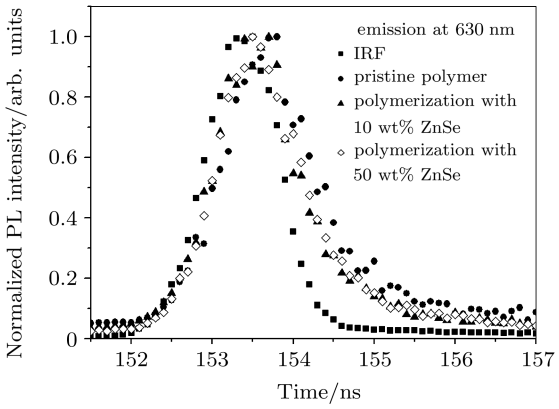


Fig. 7. Decay curves of the MOPPV polymer and the MOPPV-ZnSe thin films excited at 350 nm.

Table 1. Excited-state lifetimes, fitting to 2 exponentials for pristine polymer and to 3 exponentials for nanocomposites. Reduced chi-square is less than or equal to 1.2 and the Durbin–Watson parameter is greater than or equal to 1.7 for all samples. Percent yield is in parentheses after each decay component. Average lifetime is calculated by weighting each time component with its percentage yield. Emission wavelength is 590 nm.

emission at 590 nm film	τ_1 /ns	τ_2 /ns	τ_3 /ns	Ave.τ /ns
MOPPV	0.43(93%)	0.99(7%)		0.52
10 wt % ZnSe	0.25(61%)	0.37 (26%)	0.94(13%)	0.37
50 wt% ZnSe	0.05(77%)	0.36(21%)	1.39(1%)	0.14

Table 2. Excited-state lifetimes, fitting to 2 exponentials for pristine polymer and to 3 exponentials for nanocomposites. Reduced chi-square is less than or equal to 1.2 and the Durbin–Watson parameter is greater than or equal to 1.7 for all samples. Percent yield is shown in parentheses after each decay component. Average lifetime is calculated by weighting each time component with its percentage yield. Emission wavelength is 630 nm.

emission at 630 nm film	τ_1 /ns	τ_2 /ns	τ_3 /ns	Ave.τ /ns
MOPPV	0.56(93%)	0.56(7%)		0.56
10 wt% ZnSe	0.34(33%)	0.41(33%)	0.49(33%)	0.42
50 wt% ZnSe	0.10(82%)	0.53(17%)	1.67(1%)	0.18

shows the fast PL decay with average lifetime $\tau_{\rm av} = 0.52$ ns from a first decay time of $\tau_1 = 0.43$ ns (93%) and a tail with decay time $\tau_2 = 0.99$ ns (7%), and average lifetime $\tau_{\rm av} = 0.56$ ns from a first decay time of $\tau_1 = 0.56$ ns (93%) and a tail with decay time of $\tau_2 = 0.56$ ns (7%) below 0.8 ns at the 'blue' and the 'red' ends of the emission spectrum, respectively. This short time scale suggests the presence of multiple decay channels for intrachain excitons in conjugated polymer. This result is similar to the one for poly[2-methoxy-5-(2'-ethylhexyloxy)-1,4-phenylenevinylene](MEH-PPV) reported in Ref. [19]. On the other hand, it should be noted that the PL decay in the nanocomposite materials demonstrates a monotonic decrease in lifetime with ZnSe nanocrystal content increasing as shown in Figs. 6 and 7, respectively. Compared with the nanocomposite of the pristine polymer, the nanocomposite with 10 wt% ZnSe and 90% of the original MOPPV shows a faster PL decay with average lifetime $\tau_{\rm av} = 0.37$ ns from a first decay time of $\tau_1 = 0.25$ ns(61%) and two longer components with decay times of $\tau_2 = 0.37$ ns (26%) and $\tau_3 = 0.94$ ns(13%), and average lifetime $\tau_{\rm av} = 0.42$ ns from a first decay time of $\tau_1 = 0.34$ ns(33%) and two longer components with decay times $\tau_2 = 0.41$ ns(33%) and $\tau_3 = 0.49$ ns(33%) for both the emissions at the 'blue' and the 'red' ends as shown in Table 1 and Table 2, respectively. These findings indicate that the introduction of ZnSe nanocrystals in polymer matrix provides more interfaces for charge separation between the two components and produces a charge-separated state with an electron on the ZnSe nanocrystal and a hole on the polymer and thus the polymer emission is significantly quenched. Moreover, when the concentration of ZnSe nanocrystals in the nanocomposite is further increased (up to 50 wt%), much more surface area may be available from the efficient exciton dissociation and the charge percolation pathways may also be available from efficient charge diffusion before the occurrence of charge recombination, thereby leading polymer emission to be further quenched. Therefore, it is found that nanocomposite with 50 wt% ZnSe and 50% of the original MOPPV shows the shortest PL decay with average lifetime $\tau_{\rm av} = 0.14$ ns from a first decay time of $\tau_1 = 0.05$ ns(77%) and two longer components with decay times of $\tau_2 = 0.36$ ns (21%) and $\tau_3 = 1.39$ ns(1%), and average lifetime $\tau_{\rm av} = 0.18$ ns from a first decay time of $\tau_1 = 0.10$ ns(82%) and two longer components with decay times of $\tau_2 = 0.53$ ns(17%) and $\tau_3 = 1.67$ ns(1%) for both the emissions at the 'blue' and the 'red' end among Table 1 and Table 2, respectively. Similar investigations have also been carried out for polymer-CdSe nanocomposites.[20] Besides, the PL decay average lifetime data (Table 1 and Table 2) clearly reveal that the PL dynamics is dependent on not only the presence of concentration of ZnSe, but also emitted wavelength, and the blue portion of the emission shows a much faster decay at early time than the red portion of the emission, which is in agreement with another report.[21]

In short, the dominant mechanism of exciton quenching is the electron transfer from polymer to ZnSe, since the energy transfer process can lead the resulting bound electron-hole pairs at the heterojunction interface to be dissociated into free carriers and subsequently they are transported into the electrodes before the occurrence of their recombination, which is beneficial for solar cell performance.

4. Conclusions

We have successfully synthesized MOPPV-ZnSe nanocomposites by the mixing polymerization

method. HRTEM and TM-AFM show clearly evidence for phase segregated networks of ZnSe nanocrystals, providing a large area of interface for charge separation to occur. Time-resolved PL spectra further confirm the occurrence of charge transfer at the interface between the MOPPV and the ZnSe. We also identify the optical properties and microscopic origin of these changes of the MOPPV-ZnSe nanocomposites by UV–visible spectra, PL spectra, and Raman spectra, respectively. Finally, we demonstrate that conjugated polymer-ZnSe nanocrystal nanocomposites are ideal materials for achieving charge separation, and that at high nanocrystal concentrations both carriers may be transported through their two components, respectively. Further investigations of the role of ZnSe nanocrystals in hybrid solar cells will be published elsewhere.[22]

References

[1] Huynh W U, Dittmer J J and Alivisatos A P 2002 *Science* **295** 2425

[2] Koleilat G I, Levina L, Shukla H, Myrskog S H, Hinds S, Pattantyus-Abraham A G and Sargent E H 2008 *ACSNANO* **2** 833

[3] Feng W, Feng W Y and Wu Z 2005 *Jpn. J. Appl. Phys.* **44** 4794

[4] Tian R Y, Yang R Q, Peng J B and Cao Y 2005 *Chin. Phys.* **14** 1032

[5] Einosuke K, Seiki K, Akira O, Shinji A and Shinya M 2008 *Appl. Phys. Lett.* **92** 1733071

[6] Feng W, Xu Y L, Yi W H, Zhou F, Wang X G and Yoshino K 2003 *Chin. Phys.* **12** 426

[7] Bartholomew G P and Heeger A J 2005 *Adv. Funct. Mater.* **15** 677

[8] Skaff H, Sill K and Emrick T 2004 *J. Am. Chem. Soc.* **126** 11322

[9] Xu J, Wang J, Mitchell M, Mukherjee P, Jeffries-El M, Petrich J W and Lin Z 2007 *J. Am. Chem. Soc.* **129** 12828

[10] Lee W, Shin S, Han S H and Cho B 2008 *Appl. Phys. Lett.* **92** 193307

[11] Deng D W, Qin Y B, Yang X, Yu J S and Pan Y 2006 *J. Cryst. Growth* **296** 141

[12] Neef C J and Ferraris J P 2000 *Macromolecules* **3323** 11

[13] Yun D Q, Feng W, Wu H C, Li B M, Liu X Z, Yi W H, Qiang J F, Gao S and Yan S L 2008 *Synth. Met.* **158** 977

[14] Wu X F, Shi G Q, Zhang J X and Chen F E 2003 *J. Polym. Sci.* Part A **41** 449

[15] Mulazzi E, Ripamonti A, Wery J, Dulieu B and Lefrant S 1999 *Phys. Rev.* B **60** 16519

[16] Nikesh V V, Amit D L, Seiji K, Shinji N and Shailaja M 2006 *J. Appl. Phys.* **100** 1135201

[17] Aarab H, Baitoul M, Wery J, Almairac R, Lefrant R, Faulques E, Duvail J L and Hamedoun M 2005 *Synth. Met.* **155** 63

[18] Yang L, Wu P, Yen H, Zeng L, Zhang Q, Liu X and Gu P 2005 *Phys. Stat. Sol.* A **202** 289

[19] Smilowitz L, Hays A, Heeger A J, Wang G and Bowers J E 1993 *J. Chem. Phys.* **98** 6504

[20] Greenham N C, Peng X G and AliVisatos A P 1997 *Synth. Met.* **84** 545

[21] Ignacio B M, Alex D S and Benjamin J S 2004 *Phys. Rev.* B **69** 035204

[22] Yun D Q, Feng W, Wu H C and Yoshino K 2009 *Sol. Energy Mater. Cells* **93** 1208